Lab on a Chip

PAPER

View Article Online
View Journal | View Issue

Cite this: *Lab Chip*, 2025, **25**, 4635

A disease-inspired *in vitro* model of aortic valve stenosis to investigate the drivers of endothelial–mesenchymal transition†

Yasmin Mirzaalikhan,[ab] Austin Lai,[b] Manijeh Khanmohammadi,[ab] Chanly Chheang,[b] Azadeh Mirabedini,[c] Shadi Houshyar,[c] Jonathan Noonan,[bd] Anna M. D. Watson,[bde] Nalin Dayawansa,[bfg] Silvana Marasco,[gh] Karlheinz Peter[bdf] and Sara Baratchi *[abd]

Calcific aortic valve disease (CAVD) is the most prevalent heart valve disorder worldwide. Despite its growing clinical burden, there are currently no pharmacological treatments available to prevent or reverse disease progression; transcatheter or surgical valve replacement remains the only therapeutic option. In this study, we developed a disease-inspired *in vitro* model to investigate how mechanical and biochemical cues, specifically reduced tensile stress and enrichment of hyaluronic acid (HA) within extracellular matrices (ECM), influence valvular endothelial cell biology, both hallmark features of CAVD. To achieve this, we developed a hydrogel-based model, incorporating different concentrations of HA to mimic healthy, mild, and moderate stages of CAVD. Valvular endothelial cells were cultured on these ECM conditions and subjected to cyclic stretch at 0%, 10%, and 20%, representing static (no mechanical stimulation), physiological (healthy), and pathological (hypertensive) conditions, respectively. We found that HA enrichment within the ECM, combined with reduced stretch intensity, induced an intermediate endothelial-to-mesenchymal transition (EndMT) phenotype, as evidenced by increased expression of vWF, CD31, αSMA, and MMP9. Notably, the application of 10% and 20% cyclic stretch mitigated the pro-EndMT effects of HA enrichment. Additionally, HA enrichment and stretch intensity influenced the expression of ICAM-1, an inflammatory marker, and subsequent THP-1 monocyte adhesion. Under static conditions, HA deposition alone did not significantly affect cell adhesion. However, 10% stretch reduced ICAM-1 expression and monocyte adhesion, whereas at 20% stretch, high HA concentrations enhanced monocyte adhesion. To validate our *in vitro* findings, we analysed aortic valve tissues from CAVD patients and healthy donors. CAVD valves showed the increased CD31, MMP9, and α-SMA expression, reduced vWF levels, and heightened cellular infiltration, confirming key inflammatory and structural changes observed *in vitro*. This work establishes a physiologically relevant *in vitro* platform to study CAVD progression and highlights the importance of ECM composition and mechanical loading in modulating endothelial biology and immune interactions.

Received 17th May 2025,
Accepted 6th June 2025

DOI: 10.1039/d5lc00484e

rsc.li/loc

Introduction

Calcific aortic valve disease (CAVD) is the most common heart valve disorder globally and the third most prevalent cardiovascular disease,[1] with its incidence rising significantly among the ageing population.[2] CAVD is characterised by inflammation, fibrosis, and valvular calcification. This process leads to the gradual narrowing of the aortic valve, restricting valve area and impairing blood flow from the left ventricle to the aorta, resulting in left ventricular overload, which leads to heart failure and death if not treated.[3–5] Unfortunately, to date, there is no approved pharmacotherapy to slow or reverse the process of valve calcification, and valve replacement, either *via* surgery or transcatheter intervention,

[a] *School of Health and Biomedical Sciences, RMIT University, Melbourne, Victoria, Australia*
[b] *Baker Heart and Diabetes Institute, Melbourne, Victoria, Australia. E-mail: sara.baratchi@baker.edu.au*
[c] *School of Engineering, RMIT University, Melbourne, Victoria, Australia*
[d] *Department of Cardiometabolic Health, University of Melbourne, Parkville, Victoria, Australia*
[e] *Department of Diabetes, School of Translational Medicine, Monash University, Victoria, Australia*
[f] *Department of Cardiology, The Alfred Hospital, Melbourne, Victoria, Australia*
[g] *Central Clinical School, Monash University, Melbourne, Victoria, Australia*
[h] *Department of Cardiothoracic Surgery, The Alfred Hospital, Melbourne, Victoria, Australia*

† Electronic supplementary information (ESI) available. See DOI: https://doi.org/10.1039/d5lc00484e

remains the only treatment option. Without valve replacement, there is a 50% chance of mortality within two years of diagnosis for patients with symptomatic, severe aortic stenosis.[6–8]

Insufficient understanding of the CAVD pathophysiology is the main obstacle to developing appropriate pharmacotherapy. The aortic valve is composed of valve endothelial cells, valve interstitial cells, and extracellular matrix (ECM). The pathophysiology of the disease is complex and involves endothelial dysfunction, immune cell infiltration, endothelial-to-mesenchymal transition (EndMT), osteoblastic differentiation of valve interstitial cells, and calcification.[9,10] EndMT is vital in embryonic development and contributes to other diseases, including cancer and various cardiovascular disorders, making it a potential therapeutic target.[10,11]

The aortic valve is a highly dynamic structure, opening and closing approximately 42 million times per year. The mechanical forces that the aortic valve experiences during each cardiac cycle are characterised by circumferential tensile stress, which results in a cyclic stretch of the valve leaflets during each cardiac cycle. This mechanical stimulus is crucial in maintaining endothelial cell function and preserving valve homeostasis.[12] Under physiological conditions, healthy valve leaflets typically experience around 10% cyclic stretch, while elevated stretch levels of 15–20% are associated with hypertensive states.[13] As the CAVD progresses, the magnitude of cyclic stretch decreases due to leaflet stiffening and calcification, while the ECM undergoes remodelling and becomes enriched with glycosaminoglycans such as hyaluronic acid (HA). Also, calcification begins in areas experiencing high mechanical strain, and in calcified regions, strain decreases as calcium deposits spread.[14] In this paper, we aimed to develop a model that enables us to study the effect of changes in stretch intensity and ECM reorganisation on valvular endothelial cells, which could contribute to the progression of CAVD.

One of the most essential CAVD hallmarks is the widespread alteration in the structure and mechanical properties of the valve ECM.[15] The ECM of the mature aortic valve consists of three highly organised, overlapping layers with distinct mechanical properties, oriented according to blood flow direction. The primary components of these layers are collagen, proteoglycans, and elastin. In the aortic valve, the fibrosa layer (the aortic side of the valve) is primarily composed of collagen type I, while the spongiosa layer (the middle layer) consists of proteoglycans, and the ventricularis layer (the ventricular side) is rich in elastin.[16,17] During the CAVD development, ECM becomes enriched in glycosaminoglycans (GAGs) such as HA. Human aortic valve endothelial cells (HAoVECs) are key regulators in the early stages of CAVD, interacting with immune cells and the ECM. The disease initiation is marked by the loss of HAoVECs integrity, leading to endothelial dysfunction, lipoprotein infiltration, and immune cell recruitment, which trigger inflammation and EndMT.[18] Hemodynamic alterations, such as hypertension, age-related valvular stiffening, and oxidative stress, trigger HAoVECs injury and activation.[19] As the disease progresses, lymphocytes and monocytes infiltrate the sub-endothelium, forming lipid-laden foam cells and leading to inflammation in CAVD.[20] The ECM is a dynamic structure that undergoes remodelling during normal or pathological conditions. HA is the most prevalent component of the ECM of various tissues, such as the aortic valve, and is composed of repeating polymeric glucuronic acid and *N*-acetyl-glucosamine disaccharides.[21,22] HA is commonly used in biomaterial applications and tissue engineering. Within the matrix environment, HA interacts with its receptor CD44 and plays an important role in modulating cell proliferation, development, and adhesion.[23,24] The complexity of the native valve ECM and the limitations of histological analysis make it challenging to dissect the sequence of events in valve pathology. Therefore, engineered *in vitro* models aim to mimic key ECM features and hemodynamic characteristics to uncover critical underlying mechanisms of CAVD pathophysiology. Among ECM components, hyaluronic acid is an attractive valve-mimicking biomaterial due to its abundance and role in CAVD and EndMT.[25] While previous studies have shown that incorporating HA into collagen hydrogels—in the absence of mechanical stretch—can significantly promote EndMT and cellular invasion,[26] the combined impact of HA enrichment and physiologically relevant cyclic stretch on HAoVECs biology has not been investigated. Given that the aortic valve is a highly dynamic structure, continuously subjected to pulsatile blood flow and mechanical deformation, tensile stress on the valve leaflets plays a critical role in regulating the biology of HAoVECs, which act as mechanotransducers, converting physical stress into cellular signals. Here, we present a novel study examining the synergistic effects of HA-enriched ECM and cyclic stretch on EndMT and inflammatory activation of HAoVECs. This integrative, mechanobiology-informed approach provides new and translationally highly relevant insights into how matrix composition and mechanical forces cooperate to drive VEC dysfunction in valve disease.

Materials and methods

Preparation of hydrogel

Hydrogels were prepared in three different conditions: 1) control: 6 mg ml^{-1} methacrylated collagen I (PhotoCol; catalog no #5270 Advanced Biomatrix) (ColMA), 2) healthy: 6 mg ml^{-1} ColMA + 2 mg ml^{-1} methacrylated hyaluronic acid (PhotoHA; catalog no #5274) (ColMA + HA2), and 3) diseased: 6 mg ml^{-1} ColMA + 10 mg ml^{-1} HA (ColMA + HA10). LAP photoinitiator (at a concentration of 17 mg ml^{-1} in 1X phosphate-buffered saline (PBS)) was added, followed by blue light photo-crosslinking of the hydrogel at 405 nm for 5 min. The volume of the photoinitiator was calculated by multiplying the total volume of the hydrogel solution by 0.02. The thickness of the hydrogel used in every condition is ~1.3 mm.

Rheological characterisation of hydrogels

Frequency sweep rheometry was conducted to evaluate the viscoelastic properties and flow behaviour of ColMA-based hydrogel formulations with and without HA supplementation. Three formulations, ColMA (control), ColMA + HA2, and ColMA + HA10, were tested using a Discovery HR-3 Rheometer (TA Instruments, New Castle, DE) equipped with a 25.0 mm cone and plate geometry (2°) system (ETC Steel, 118288) and Peltier temperature control system set to 37 °C to simulate physiological conditions. The hydrogels were UV-cured *in situ* on the Peltier plate to

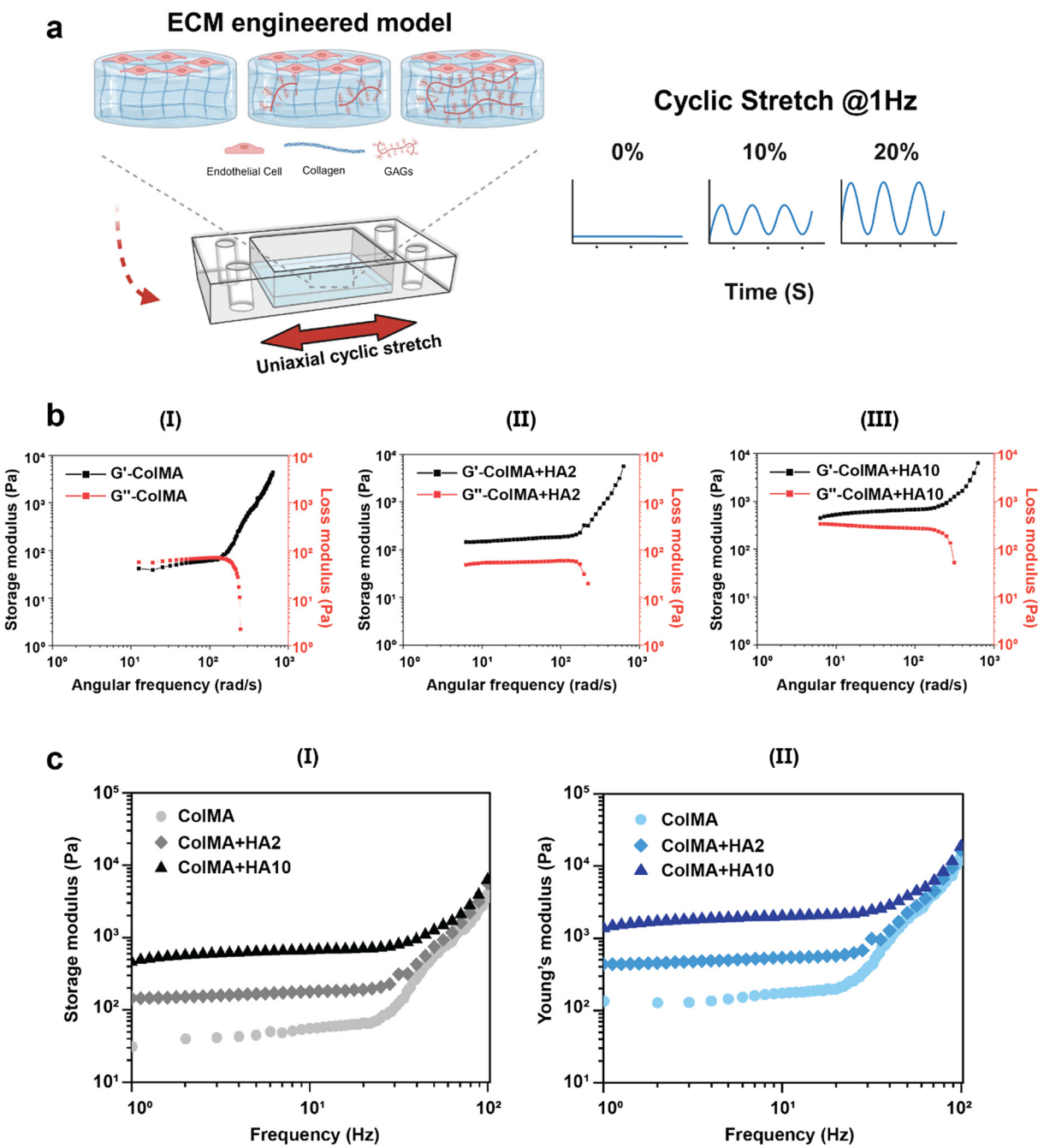

Fig. 1 Hyaluronic acid in the ECM modulates the mechanical properties of the hydrogel. (a) Schematic representation of the three different hydrogel conditions used. ($1b_{I–III}$) frequency-dependent storage (G') and loss (G'') moduli for (b_I) ColMA, (b_{II}) ColMA + HA2, and (b_{III}) ColMA + HA10 hydrogels. Each subpanel shows G' (black symbols) and G'' (red symbols) *vs.* angular frequency. ($c_{I\ and\ II}$) Viscoelastic moduli of ColMA hydrogels with increasing HA content, plotted against linear frequency (Hz). (c_I) Storage modulus (G') for pure ColMA, ColMA + HA2 (mid-tone ◆), and ColMA + HA10 (black ▲). (c_{II}) Corresponding Young's modulus $E'(\omega)$ (in compression/tension) estimated from G' (assuming near-incompressibility) for ColMA (light blue ●), ColMA + HA2 (blue ◆), and ColMA + HA10 (dark blue ▲). The Fig. 1a was created using **https://BioRender.com** and is licensed under BioRender's academic license.

ensure uniform crosslinking and consistent testing conditions.

Frequency sweep measurements were performed from 1–100 Hz at a set strain of 20% to determine key rheological properties, including storage modulus (G') and loss modulus (G''). In addition, the Young's modulus was calculated from G' at each frequency using the equation $E = 2G'(1 + \nu)$, assuming a Poisson's ratio (ν) of ~0.5, with results plotted as a function of frequency to illustrate the elastic response of each formulation under dynamic loading.

Cell culture

HAoVECs (catalog #00225975 Lonza) were obtained and subcultured in EGM™-2 endothelial cell growth medium-2 BulletKit™ (catalog #CC-3162 Lonza). Cells between passages 4–8 were used in this study. HAoVECs were seeded on top of the fibronectin-coated hydrogels at a density of 80 000 cells per well for 24 hours and at 37 °C in a humidified incubator with 5% CO_2 to allow the endothelial cells to adhere. THP-1 cells were obtained from ATCC and maintained in RPMI 1640 medium containing 10% fetal bovine serum (Life Technologies), 1% penicillin–streptomycin (Life Technologies), 10 mM HEPES buffer (Life Technologies), and 2 mM L-glutamine (Life Technologies).

Exposure of endothelial cells to cyclic stretch

To expose the endothelial cells to a defined level of cyclic stretch, deformable multi-well PDMS stretch chambers (SC-0044-Strex) were used. Hydrogels were polymerised directly inside the PDMS chambers, where they adhered to the chamber surface. After polymerisation, human aortic valve endothelial cells were seeded on top of the hydrogels for 24 hours to allow endothelial cells to form a confluent monolayer (Fig. 1a). Following that, stretch chambers were placed in the chamber bracket of the stretching system (ST-1400, STREX) and were subjected to a cyclic stretch of 10% and 20% at 1 Hz for 16 h inside the cell culture incubator at 37 °C. Static chambers were left in the incubator at 37 °C. To confirm that endothelial cells experienced mechanical stretch, cytoskeletal alignment was assessed post-stretch by staining F-actin with phalloidin and imaging *via* confocal microscopy.

Immunofluorescent staining and confocal microscopy of hydrogels

After each experiment, cells on hydrogels were fixed using 4% paraformaldehyde (PFA), pH 7.4 in PBS for 1 h at 37 °C, followed by 3 washes with PBS (Gibco, pH 7.4) and permeabilised with 0.1% Triton X-100 (Sigma-Aldrich) for 10 min at room temperature. Next, cells were blocked with 10% goat serum for 1 hour at 37 °C followed by staining with primary antibodies, mouse anti-CD31 monoclonal antibody (Invitrogen, #BMS137, 1 : 200), rabbit anti-MMP9 monoclonal antibody (Invitrogen, #MA5-32705, 1 : 200), rabbit anti-vWF polyclonal antibody (Sigma, #F3520, 1 : 200), mouse anti-alpha-smooth-muscle actin monoclonal antibody (Invitrogen, #14-9760-82 1 : 200), and mouse anti-ICAM1 antibody (Abcam, #ab2213 1 : 200). The secondary antibody staining was performed using Alexa-647-goat anti-mouse, Alexa-647-goat anti-rabbit, Alexa-488-goat anti-mouse, and Alexa-488-goat anti-rabbit antibodies (all from Invitrogen, 1/400). F-actin was stained with Atto 565-phalloidin (Sigma-Aldrich, 1/1000), and the nuclei were stained with DAPI (Thermo Scientific, 1/400). Images were acquired using a Nikon A1 confocal microscope (Nikon, Japan) equipped with either 10× or 20× objective lenses and 2–4× camera zoom.

MMP activity

The overall activity of matrix metalloproteinases (MMPs) was measured using a fluorescence-based MMP activity assay according to the manufacturer's instructions (Abcam, #ab112146). Briefly, cell lysates were prepared and centrifuged at 12000 rpm for 10 min, and MMP green substrate and 10 μg of cell lysate protein were added to a 96-well plate. Fluorescence was measured at an excitation/emission of 490/525 nm.

Cell adhesion assay

To assess THP-1 adhesion to valve endothelial cells, THP-1 cells were labelled with LeukoTracker Green (Cell Biolabs) for 15 minutes at 37 °C, then washed with PBS to remove excess dye, following the supplier's instructions. The labelled THP-1 cell suspension was then perfused over a monolayer of endothelial cells that had been exposed to different levels of cyclic stretch overnight, at a 3 : 1 ratio (THP-1 to endothelial cells).

Ethic statement

All experiments were performed in accordance with the Guidelines of the Alfred Human Ethics Committee, and the recruitment of the human aortic valve biospecimens was performed following approval from the Alfred Hospital Ethics Committee (project 560/1). Informed consents were obtained from human participants of this study.

Human aortic valve samples and immunohistochemistry (IHC)

Calcified human aortic valve tissue was obtained from patients undergoing surgical valve replacement at The Alfred Hospital, Melbourne, Australia. Non-calcified human aortic valves were obtained from deceased Australian organ donors from the Australian Donor Tissue Biobank. All studies involving human biospecimens were approved by the Alfred Research Ethics Committee. Fresh tissues were immediately embedded in optimal cutting-temperature compound and frozen at −80 °C (Tissue-Tek®, Sakura Finetek, The Netherlands). The study was approved by the Alfred Hospital Ethics Committee. Serial 6 μm

sections were prepared using a cryostat (cryostat, Leica CM1950). Fresh frozen tissue sections were cut, air-dried for 60 min, and stored at −20 °C. Before staining, sections were fixed in 95% ethanol, 100% ethanol, cold acetone, and air dried for 20–30 min, followed by fixation in 4% PFA for 15 min. After blocking with 10% goat serum and 5% BSA for 30 min, primary antibodies targeting specific markers Ms-CD31 (Invitrogen, #BMS137 1 : 200), Rb-MMP9 (Invitrogen, #MA5-32705 1 : 200), Ms-αSMA (Invitrogen, #14-9760-82 1 : 200), Ms-ICAM1 (Abcam, #ab2213), and Rb-vWF (Sigma, #F3520 1 : 200) were applied overnight at 4 °C. Sections were then incubated with secondary antibodies (Alexa-647 conjugated goat anti-mouse and Alexa-488 conjugated goat anti-rabbit antibodies (both from Invitrogen)) for 2–3 h, followed by staining with CD62P-568 (Biosciences #348107) and DAPI. Sections were mounted in ProLong Gold antifade mountant and stored at 4 °C until imaging. Imaging was performed using a Zeiss Axioscan 7.

Data analysis

The orientation of actin stress fibres was analysed using a custom MATLAB script, as described in detail elsewhere.[27] Cell areas were determined by drawing regions of interest (ROIs) around individual cells and using the area measurement functions in NIS-Elements software (Nikon Instruments Inc.). The cell aspect ratio was calculated by measuring the long and short axes of endothelial cells, also using NIS-Elements.

The nucleus area was determined from a thresholded DAPI-stained image using the 'analyse particle' function on ImageJ (v. 1.54). To assess the expression of different inflammatory and EndMT markers, we analysed at least 20 cells from each of the 12 randomly selected fields per condition across four independent experiments. For this, regions of interest (ROIs) were drawn around individual cells using NIS Elements software, and the maximum fluorescence intensity of each ROI was measured.

To evaluate marker expression across the endothelium in valve specimens obtained from patients with severe aortic stenosis or from healthy donors, we first labelled the endothelium with CD31. We then used Zeiss ZEN software to measure the intensity of the targeted markers across at least 30 regions of the valve endothelial layer.

Statistical analysis

Statistical analysis will be performed using GraphPad Prism (Version 9.0, GraphPad Software Inc., San Diego, California). Data are expressed as mean ± standard error of the mean (SEM). Significance will be determined using a standard two-way ANOVA with multiple comparison tests, with significance levels indicated as $*p < 0.05$, $**p < 0.01$, $***p < 0.001$, and $****p < 0.0001$.

Results

HA supplementation modulates the mechanical properties of the ColMA-based hydrogels

The dynamic mechanical properties of ColMA-based hydrogels, with and without HA supplementation, evaluated *via* frequency sweep rheometry performed from 1 to 100 Hz at a constant strain amplitude of 20%, are demonstrated in Fig. 1. All ColMA-based hydrogels showed typical viscoelastic solid behaviour, with G' exceeding G'' over the tested frequency range, confirming the formation of a crosslinked network (Fig. $1b_{I–III}$). However, the magnitude of G', the gap between G' and G'', and the frequency-dependence of the moduli were strongly influenced by HA concentration. Pure ColMA hydrogel exhibited the lowest G' (~10^2 Pa at 1 rad s^{-1}) and a loss tangent ($\tan\delta = G''/G'$) approaching unity at the lowest frequencies, indicating a considerable viscous component. In contrast, the ColMA-HA hybrid hydrogels, especially at the highest HA content (ColMA + HA10), showed dramatically higher G' and much smaller $\tan\delta$ (~0.1 or less), reflecting predominantly elastic behaviour. These trends suggest that incorporating methacrylated HA reinforces the collagen network, increasing its solid-like character. This result aligns with other findings that HA substantially improves the rigidity and viscoelasticity of hydrogels when crosslinked, compared to unmodified HA.[28] Lan *et al.* recently reported that pure ColMA hydrogels have a relatively small G'–G'' difference, whereas adding a second polymer network (*e.g.* tyramine-modified HA or PEGDA) raises G' and amplifies the G'–G''. Here, the ColMA + HA10 formulation displays the largest G'–G'' gap (Fig. $1b_{III}$), consistent with a more highly crosslinked or entangled dual-network that resists viscoelastic deformation.[29] Furthermore, after photopolymerisation, such dual-network hydrogels tend to show only weak frequency dependence of G' and G'', resulting in plateau-like behaviour. In our hybrids, G' remains relatively flat through mid-range frequencies compared to pure ColMA, which exhibits a more pronounced rise in G' with frequency.

Further quantitative analysis revealed a pronounced concentration-dependent increase in hydrogel stiffness upon HA incorporation. At 1 Hz, the storage modulus (G') was approximately 173 Pa for ColMA, 459 Pa for ColMA + HA2, and 642 Pa for ColMA + HA10, while at 100 Hz, G' increased to 4423 Pa, 5600 Pa, and 6283 Pa, respectively (Fig. $1c_I$). This trend reflects a 3–4-fold enhancement in shear stiffness with 10 mg ml^{-1} HA supplementation, consistent with findings reported by Gennari *et al.* on HA–collagen hybrid systems where G' increased by an order of magnitude with HA concentrations ≥5% w/v.[30] The increasing G' values across frequency (1–100 Hz) show improved crosslinking and network rigidity, with ColMA + HA10 reaching a plateau near 6.3 kPa. Young's modulus followed a similar trend: at 100 Hz, ColMA measured ~13.3 kPa, while HA2 and HA10 formulations reached ~16.8 kPa and ~18.8 kPa, respectively (Fig. $1c_{II}$ and Table S1†). These values place ColMA in the

range of soft tissues (*e.g.*, brain), and HA-supplemented variants nearer to connective tissues like dermis or relaxed muscle (10–20 kPa), making them more suitable for load-bearing applications.[31] Additionally, the reduced loss tangent (G''/G') in HA-rich gels suggests diminished viscous dissipation and a shift toward elastic-dominated behaviour. These findings align with the mechanical profiles of interpenetrating networks, where HA contributes additional

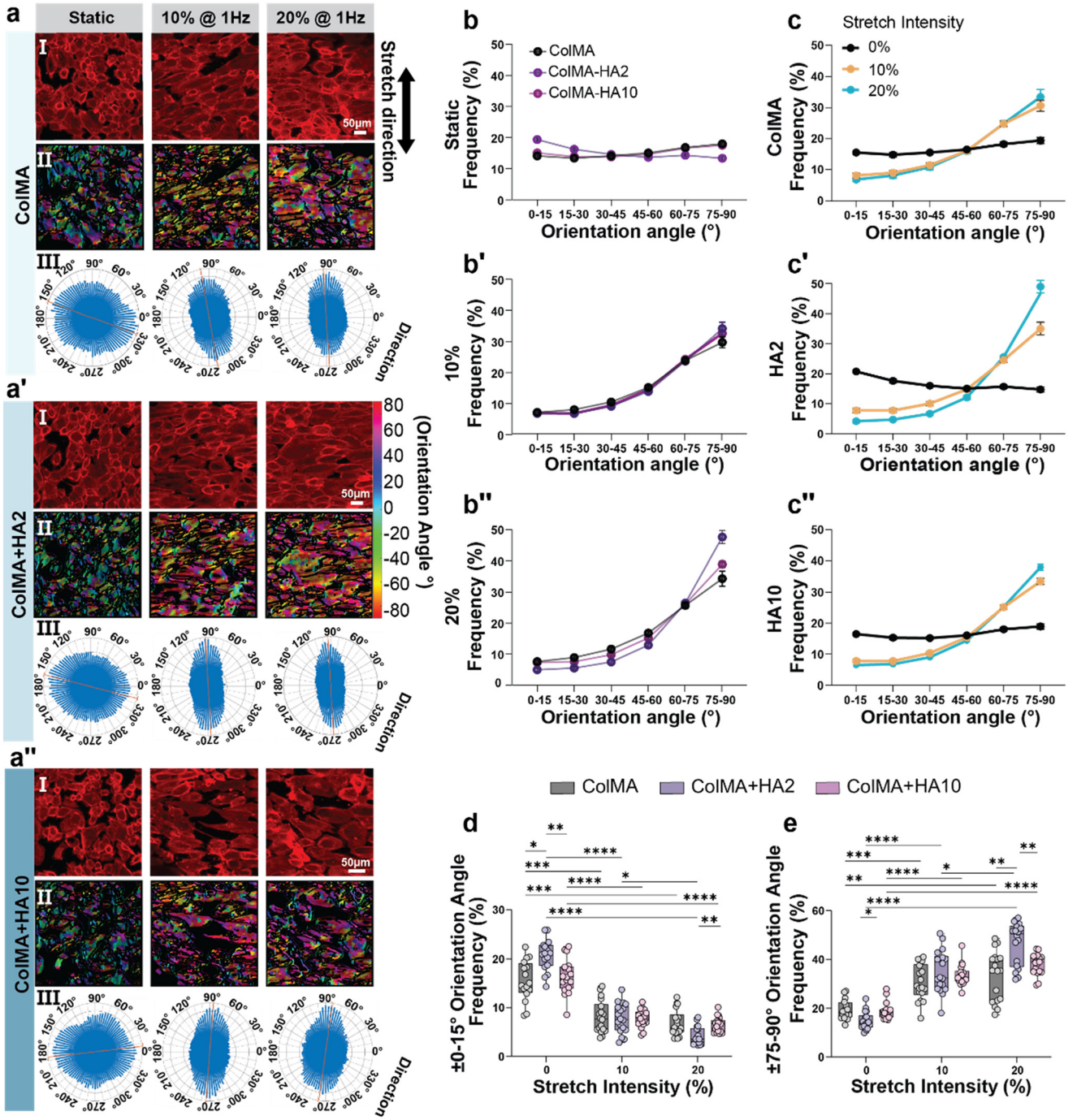

Fig. 2 Cyclic stretch affects stress fibre orientation in HAoVECs independent of the ECM environment. (a and a″) Representative images of HAoVECs stained for (I) actin filaments, (II) along with corresponding histograms showing the distribution of stress fibre orientation angles and (III) polar histograms highlighting the dominant orientation angle, demonstrate the effect of static, 10%, and 20% cyclic stretch on stress fibre alignment in cells cultured on different hydrogel substrates. (b and c) Line graphs show the frequency of orientation angle of HAoVECs's actin stress fibres cultured under different (b) stretch levels and (c) hydrogels. (d and e) Bar graphs show the frequency of stress fibres with (d) 0–15° and (e) 75–90° orientation angles in different hydrogels and stretch levels. Data is representative of 4 independent experiments. Each dot in d and e is representative of a randomly selected field of view per experiment. At least 20 cells have been analysed per field of view. Data were analysed using two-way ANOVA followed by Tukey's multiple comparisons test (*$P < 0.05$, **$P < 0.01$, ***$P < 0.001$, ****$P < 0.0001$).

cross-links, enhancing energy dissipation and thereby reinforcing the composite hydrogel.[32] The observed frequency insensitivity of G' in ColMA + HA10 may also support the presence of a well-structured and stable network, confirming the mechanical tunability of these hydrogels for targeted tissue engineering applications.

Cyclic stretch modulates the morphology of endothelial cells and the cell nucleus, independent of the ECM environment

Endothelial cells are highly mechanosensitive, responding to forces generated by blood flow and valve movement through the activation of mechanotransduction pathways. These pathways drive morphological alterations, cytoskeleton remodelling and alignment to the direction of applied force.[33–36] Importantly, changes in the extracellular matrix composition, such as enrichment of glycosaminoglycan content, can further influence endothelial mechanosensitivity.

Therefore, initially, we examined how varying stretch intensity and the hydrogel environment affect their morphology and cytoskeleton remodelling. To mimic different stages of ECM remodelling characteristics of diseased valves, we fabricated collagen hydrogels with varying concentrations of hyaluronic acid: 2 mg ml^{-1} to represent the healthy group, 10 mg ml^{-1} as the disease group, and collagen-only hydrogels as the control group for HA.[37,38] Following this, endothelial cells were cultured on top of the hydrogel and subjected to either 10% or 20% cyclic stretch, representing physiological and pathophysiological conditions, respectively. Immunostaining of the actin cytoskeleton, followed by fluorescence microscopy, was performed to assess cytoskeletal organisation.

Our findings indicate that endothelial cells exposed to 10% and 20% cyclic stretch exhibited a distinct, stress-dependent realignment of actin fibres perpendicular to the stretch direction (Fig. 2a and a^2). For example, increasing the stretch level from 0 to 10% and 20% reduced the frequency of actin stress fibres with a 0–15° orientation 0.5 ± 0.4-fold ($P < 0.001$) and 0.4 ± 0.2-fold ($P < 0.001$) while the percentage of actin fibres oriented at 75–90° showed an opposite trend 1.4 ± 0.5-fold ($P < 0.001$) and 1.6 ± 0.8-fold ($P < 0.01$) (Fig. 2d and e). Notably, the response appeared to saturate at 10% stretch, with no further significant effect on the action alignment observed between the 10% and 20% stretch levels (Fig. 2b and b^2). However, varying HA levels in the hydrogels did not influence actin stress fibre alignment (Fig. 2c and c^2), demonstrating that mechanical forces are the primary drivers of cytoskeletal alignment in this model.

We then examined the combined effects of cyclic stretch and ECM condition on endothelial cells' area, nuclear area, and cell aspect ratio (Fig. 3a and a″). Endothelial cells subjected to cyclic stretch demonstrated an increase in cell aspect ratio, whereas no major significant difference exists between those cultured on different substrates (Fig. 3b). For example, the application of 10% and 20% cyclic stretch on ColMA led to 1.6 ± 0.9-fold ($P < 0.0001$) and 1.6 ± 0.6-fold ($P < 0.0001$) increase in cell aspect ratio, consistent with stress fibre data, while no significant difference was observed between different ECM conditions of the same stretch intensity. Assessing cell area, we observed that in endothelial cells cultured under 10% stretch, an increase in HA concentration led to a 1.3 ± 0.6-fold increase in cell area ($p < 0.01$) when comparing ColMA to ColMA + HA10. However, this response was saturated at 20% stretch. Evaluating the different stretch groups, we found that the presence of HA enhanced the response to cyclic stretch with respect to cell area. For example, in endothelial cells cultured on ColMA + HA2, increasing the stretch from 0% to 20% stretch yielded a 1.3 ± 0.7-fold ($P < 0.05$) increase compared to the static group (Fig. 3c). Assessing the nucleus size, we found that endothelial cells cultured on ColMA in response to stretch intensity increased the nucleus area, while for both ColMA + HA2 and ColMA + HA10, cyclic stretch did not affect the nucleus area (Fig. 3d).

HA enrichment and cyclic stretch control EndMT in valvular endothelial cells

EndMT is a differentiation process in which endothelial cells progressively acquire the functional properties and characteristics of mesenchymal cells and express both mesenchymal and endothelial cell markers.[39,40] Numerous reports have demonstrated that EndMT and epithelial-to-mesenchymal transition are key regulators in common human diseases, including lung fibrosis and cardiovascular diseases.[41,42] In particular, EndMT is necessary for valve development at the embryonic stage, and adult valvular endothelial cells might also re-experience this cellular reprogramming, contributing to the abnormal stiffening and calcification of the aortic valve.[43]

Therefore, we asked whether the enrichment of HA in the ECM environment would induce EndMT and whether mechanical forces regulate this process. For this, we assessed the expression of CD31 and vWF as endothelial markers and MMP9 and α-SMA as mesenchymal markers (Fig. 4 and S1†).

Assessing the expression of CD31 and vWF, we observed that under static conditions, increasing the concentration of HA in the ECM from 0 (ColMA) to 10 mg ml^{-1} (ColMA-HA10) resulted in a significant elevation in the expression of both markers: 4.2 ± 4.4-fold ($P < 0.01$) for CD31 and 26.15 ± 47.8-fold ($P < 0.001$) for vWF. We noted a similar trend while evaluating the expression of vWF and MMP9. Furthermore, we found that exposing cells to cyclic stretch counteracts this effect (Fig. 4a and b). Under static conditions, increasing the concentration of HA from 0 (ColMA) to 10 mg ml^{-1} (ColMA – HA10) led to a significant increase in the expression of MMP9 (13 ± 102.5-fold, $P < 0.05$) and αSMA (2 ± 2.1-fold, $P < 0.01$). Similar to the endothelial markers, exposure of endothelial cells to cyclic stretch attenuated the HA-induced upregulation of MMP9 and αSMA. For instance, in

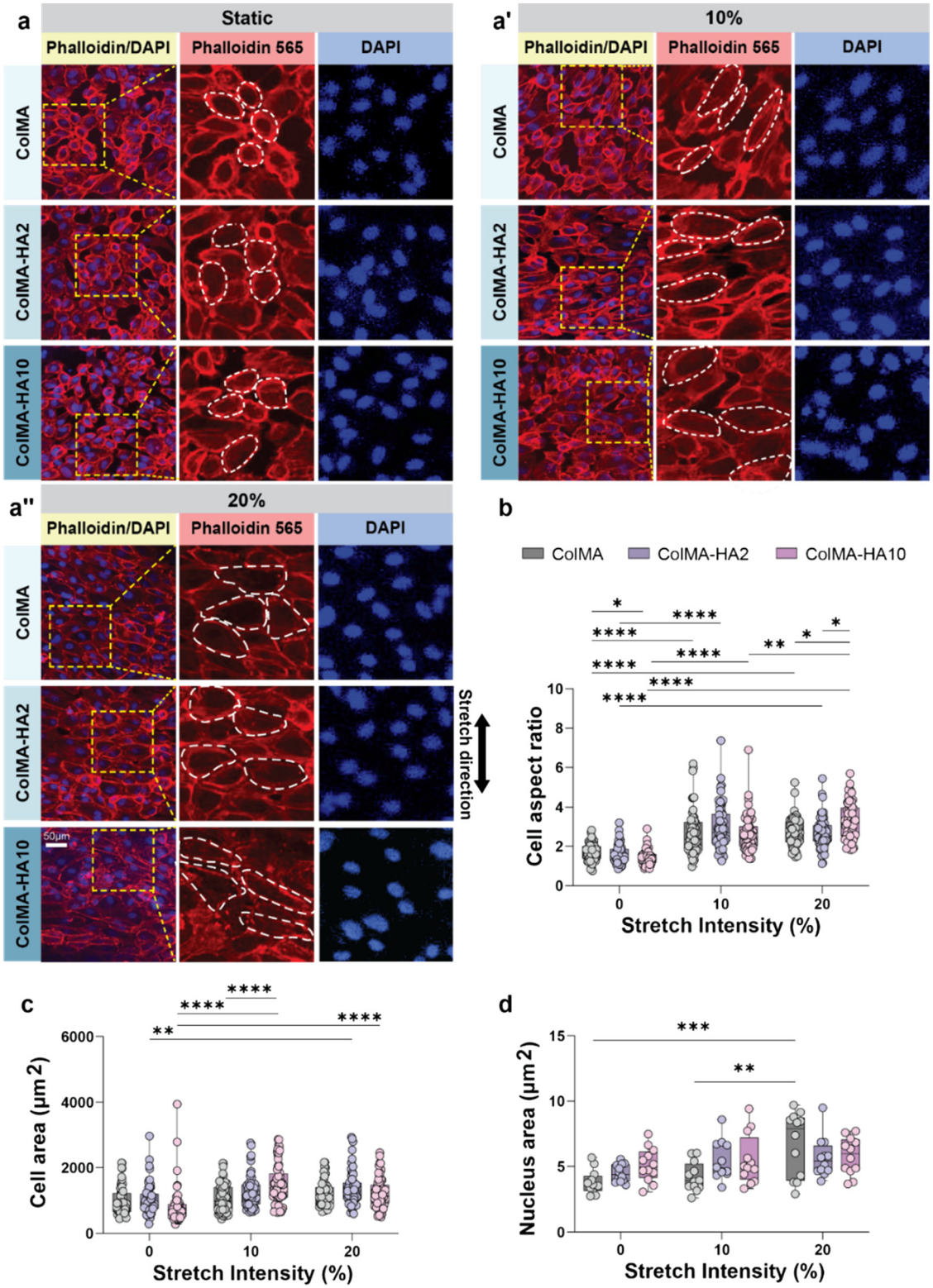

Fig. 3 Cyclic stretch changes the morphology of endothelial cells and the cell nucleus. (a and a″) Representative images of HAoVECs labelled with phalloidin (red) and DAPI (blue) show cell morphology and nuclear size under different hydrogels and cyclic stretch levels, with dashed lines indicating cell area. Bar graphs represent (b) the cell ratio, (c) the cell area, and (d) the nuclear area of HAoVECs cultured on ColMA, ColMA supplemented with 2 mg ml^{-1} HA, or 10 mg ml^{-1} HA, with or without exposure to 10% or 20% cyclic stretch. Data is representative of 4 independent experiments. Each dot in bar graphs b–d is representative of randomly selected field of view per experiment. At least 20 cells have been analysed per field of view. Data were analysed using two-way ANOVA with Tukey's test (*$P < 0.05$, **$P < 0.01$, ***$P < 0.001$, ****$P < 0.0001$).

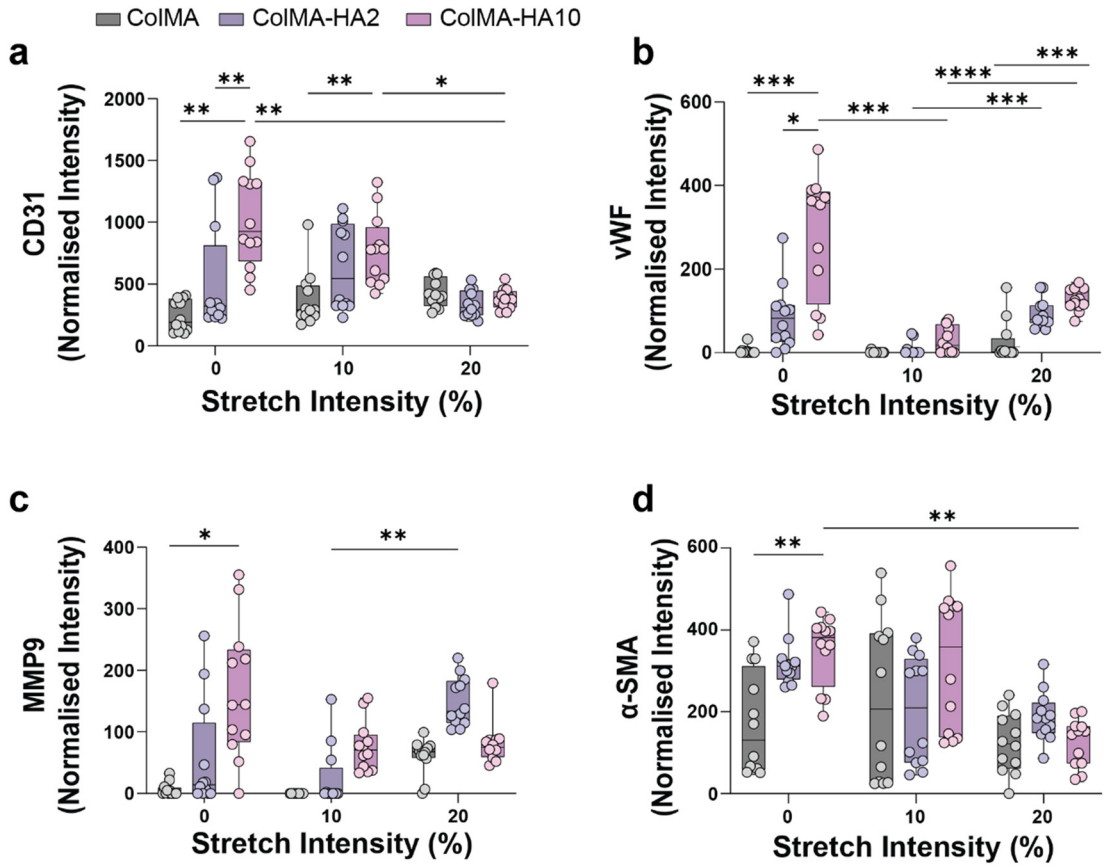

Fig. 4 Increased enrichment of HA in the absence of stretch increases the expression of EndMT markers. The expression of endothelial and mesenchymal markers in HAoVECs cultured on different hydrogels for 24 hours, followed by overnight cyclic stretch, reveals the effects of HA deposition and cyclic stretch on EndMT. (a–d) Bar graphs showing the normalised intensity of (a) CD31, (b) vWF, (c) MMP9 and (d) α-SMA in HAoVECs cultured on ColMA, ColMA + HA2 and ColMA + HA10 in the presence or absence of 10% and 20% cyclic stretch. Data is representative of 4 independent experiments. Each dot is representative of a randomly selected field of view per experiment. At least 20 cells have been analysed per field of view. Graphs were analysed using two-way ANOVA followed by Tukey's multiple comparisons test (*$P < 0.05$, **$P < 0.01$, ***$P < 0.001$, ****$P < 0.0001$).

endothelial cells cultured in ColMA − HA10, exposure to 20% cyclic stretch led to a 0.3 ± 0.2-fold ($P < 0.01$) decrease in the expression of αSMA compared to the static group. These findings demonstrate that increased HA concentration in the ECM, combined with reduced levels of mechanical stress, promotes EndMT in endothelial cells (Fig. 4c and d). We also assessed the total MMP activity in both cell lysates using an ELISA kit at different time points in ColMA and ColMA − HA10 under various stretch conditions; however, no significant differences were observed between the stretch groups (Fig. S2†), likely due to regulatory mechanisms such as TIMP inhibition or lack of MMP activation.[44]

GAGs deposition and cyclic stretch regulate inflammation and THP-1 adhesion to endothelial cells

Next, we assess the effect of an increase in HA concentration in the presence or absence of cyclic stretch on the expression of the inflammatory marker, ICAM1, and the adhesion of THP1 to endothelial cells (Fig. 5). Assessing the expression level of ICAM1, we found that under static conditions, an increase in the concentration of HA from 0 (ColMA) to 10 mg ml^{-1} (ColMA − HA10) in the ECM led to an increase in the expression of ICAM1 by 1.6 ± 24-fold ($P < 0.01$). Also, increasing the stretch intensity from 10% to 20% in endothelial cells cultured on ECM with 10 mg ml^{-1} HA, led to an increase in the expression of ICAM-1 by 2 ± 1-fold ($P < 0.05$) (Fig. 5b). Assessing the number of THP-1 cells adhered to endothelial cells, we found that exposure to 10% cyclic stretch for all ECM conditions led to a significant decrease in the number of THP-1 cells attached to endothelial cells compared to the static group ($P < 0.01$). Furthermore, in the presence of 20% cyclic stretch, an increase in HA concentration to 10 mg ml^{-1} (ColMA − HA10) led to a 3.5 ± 3.2-fold increase in the number of adhered THP-1 cells compared to ColMA (Fig. 5c). Interestingly, under 10% cyclic stretch, an increase in HA concentration did not elevate ICAM-1 expression or THP-1 adhesion. These findings suggest that physiological levels of mechanical stretch may exert a protective or stabilising effect on the endothelial phenotype by attenuating inflammatory activation. This

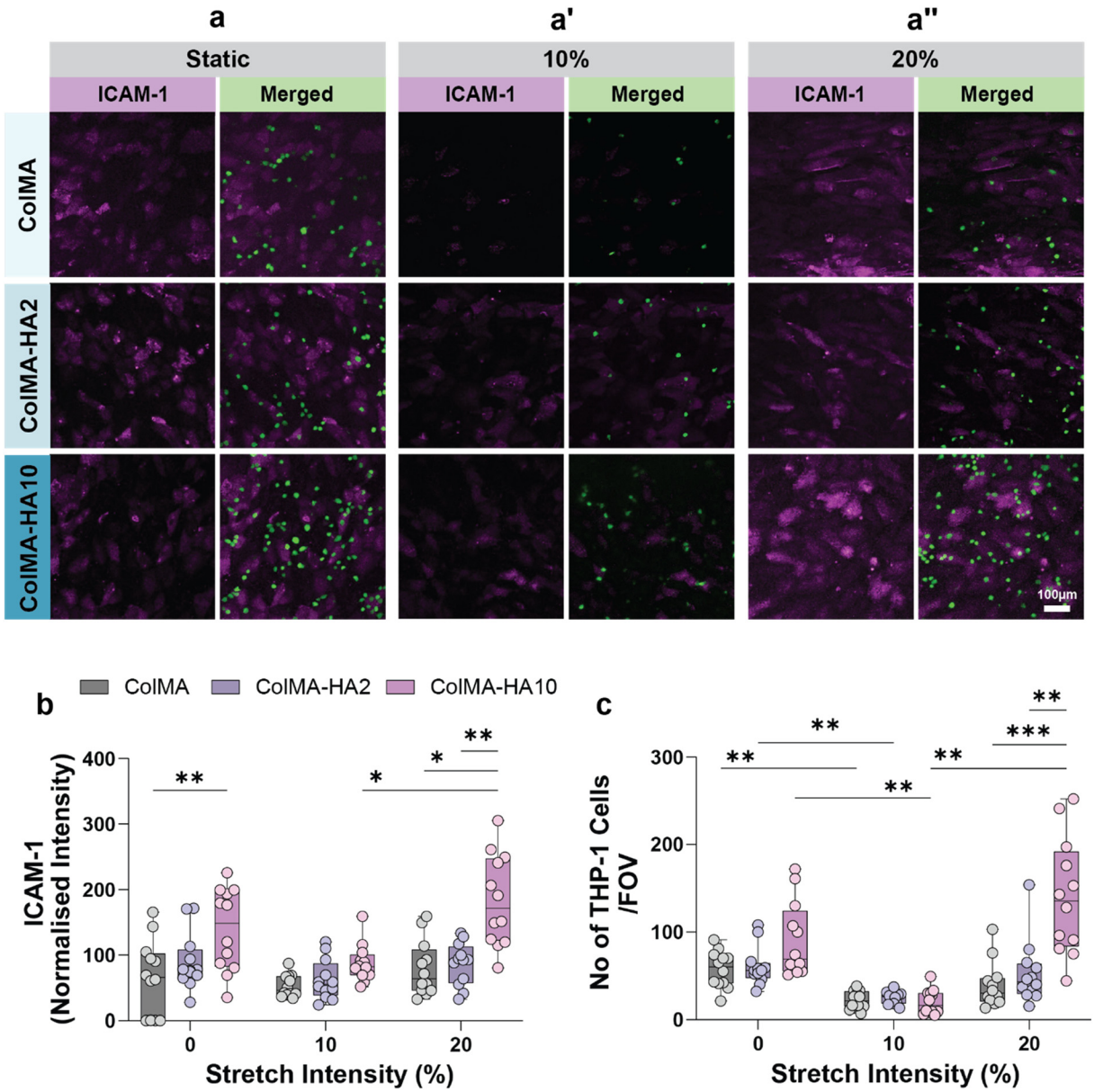

Fig. 5 Monocyte adhesion and ICAM-1 expression are regulated by HA enrichment and cyclic stretch. (a and a^2) Representative images of labelled THP-1 cells (green) adhered to endothelial cells cultured on different hydrogels, either under static conditions or subjected to 10–20% cyclic stretch, stained for ICAM-1. (b) Bar graphs show the normalised ICAM-1 expression in HAoVECs cultured on ColMA, ColMA + HA2, and ColMA + HA10 in the presence or absence of 10% and 20% cyclic stretch, and (c) the number of THP-1 cells adhered to endothelial cells per field of view. Data is representative of 4 independent experiments. Each dot in b and c is representative of a randomly selected field of view per experiment. At least 20 cells have been analysed per field of view. Graphs were analysed using two-way ANOVA, mixed-effect analysis, and multiple comparison tests (*$P < 0.05$, **$P < 0.01$, ***$P < 0.001$).

observation aligns with previous reports indicating that physiological mechanical strain supports endothelial homeostasis and survival, in part by promoting cell alignment and minimising detrimental stress on the endothelium.[45] This protective effect is similar to the atheroprotective effect of physiological levels of laminar shear stress.[46] This finding is consistent with the increase in the expression of ICAM-1 and vWF in response to HA concentration in the ECM and cyclic stretch and demonstrates that both ECM signalling and mechanotransduction control endothelial activation and the inflammatory phenotype.

Altered expression of EndMT markers in calcific *versus* healthy human aortic valves

To validate our *in vitro* findings, we analysed diseased aortic valve leaflets removed from patients with CAVD undergoing surgical valve replacement and compared them to healthy aortic valves obtained from deceased organ donors without

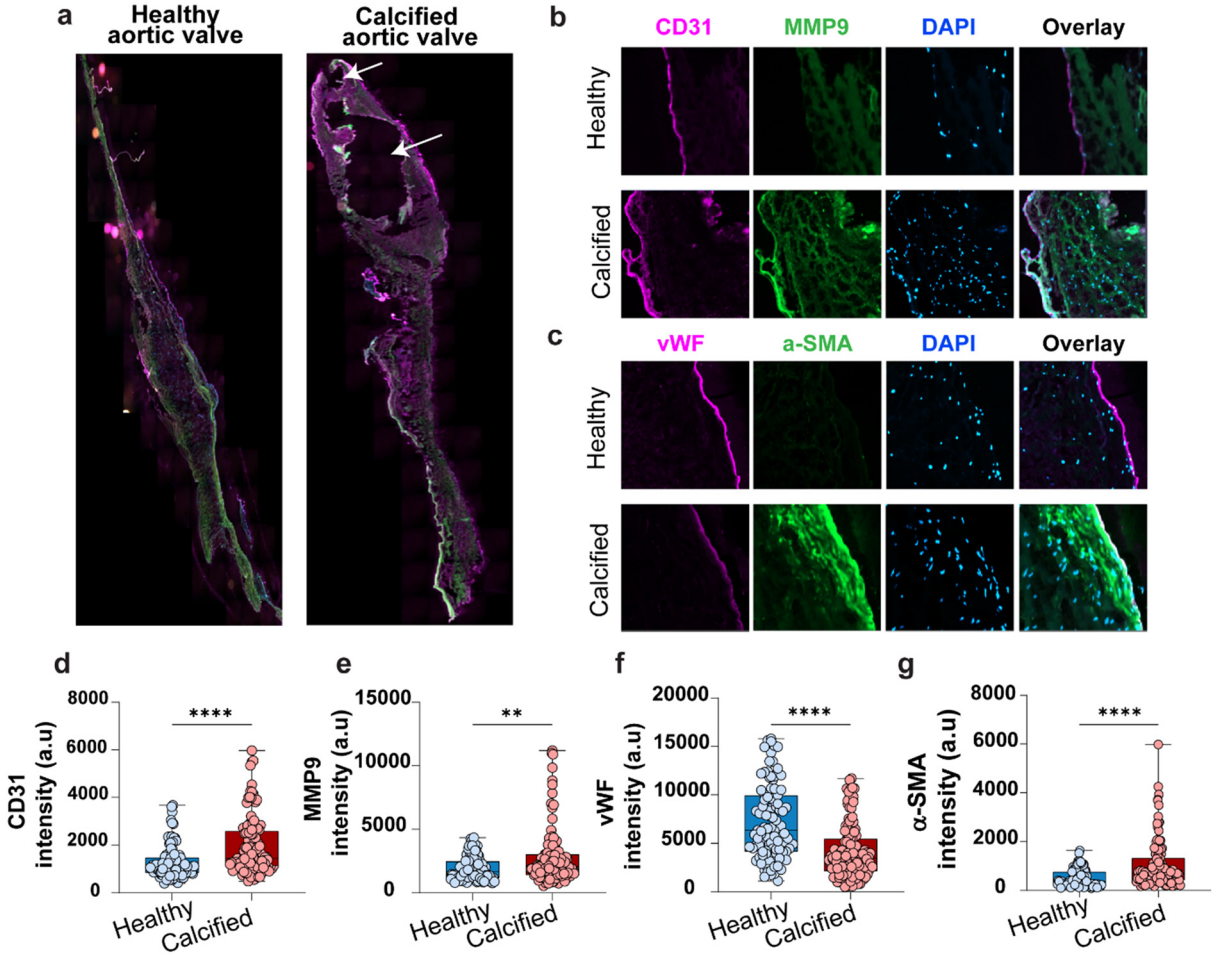

Fig. 6 EndMT marker expression is altered in aortic valve tissue in patients with severe CAVD compared to patients in healthy controls. Representative images of IHC staining of healthy and calcified aortic valve tissues showing (a) full sections and (b and c) zoomed selected areas stained for EndMT markers throughout the endothelium layer. The bar graphs show the expression levels of (d) CD31, (e) MMP9, (f) vWF, and (g) α-SMA across the endothelium in CAVD tissue compared to healthy controls. Each dot represented a randomly selected field of view based on the expression of CD31 from 4 independent donors (N = 4 valve tissues and n = 30 per tissue). Data were analysed using a non-parametric Mann–Whitney U test (**$P < 0.01$, ***$P < 0.001$, ****$P < 0.0001$).

CAVD. Morphologically, the calcified valves were thicker and exhibited prominent calcium nodules highlighted by white arrows (Fig. 6a).

We performed immunofluorescence staining, using CD31 to label the endothelial layer, and assessed the expression of CD31, MMP9 (Fig. 6b), von Willebrand Factor (vWF), and α-smooth muscle actin (α-SMA) (Fig. 6c) across multiple regions of the endothelium on both the aortic and ventricular sides of the valves. Quantitative analysis revealed that expression of CD31 and MMP9 was 1.5 ± 1.2-fold and 1.4 ± 0.9-fold higher, respectively, in CAVD valves compared to healthy specimens (Fig. 6d and e). Additionally, α-SMA expression was elevated by 2 ± 4.4-fold in CAVD valves, whereas vWF expression was reduced to 0.5 ± 1-fold relative to healthy controls (Fig. 6f and g).

Consistent with an inflammatory microenvironment, CAVD valves also showed increased levels of cellular infiltrates, as indicated by denser DAPI nuclear staining in Fig. 6b and c.

Discussion and conclusions

CAVD represents a significant and growing health burden in the ageing population, with no current pharmacological treatments capable of halting or reversing its progression. Recent studies have identified EndMT as a critical contributor to the pathogenesis of CAVD, yet the mechanistic drivers of this process remain poorly understood. Developing a bioengineering model that accurately recapitulates the mechanical and biochemical environment of the diseased valve is therefore essential for advancing our understanding of EndMT and for identifying potential therapeutic targets.

EndMT is a process where endothelial cells lose their endothelial phenotype and acquire mesenchymal characteristics, including increased proliferation, increased secretion of various molecules such as ECM proteins, loss of cell–cell junctions, elongated morphology, and increased migration, which can consequently contribute to CAVD.[47–50]

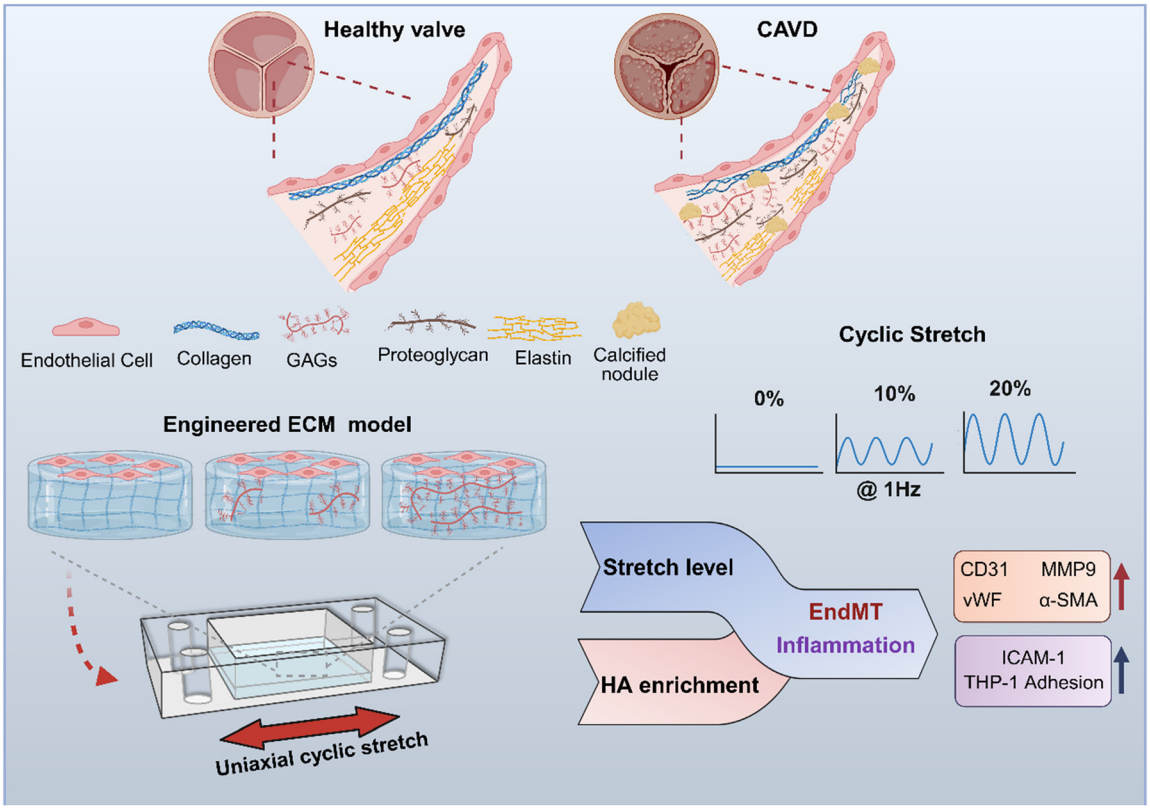

Fig. 7 A summary diagram depicting the progression of CAVD, highlighting how reduced stretch intensity and HA enrichment within the aortic valve leaflets drive EndMT and trigger endothelial inflammation. This figure was created using **https://BioRender.com** and is licensed under BioRender's academic license.

During EndMT, cells express both endothelial and mesenchymal markers, a key feature of this process. Thus, EndMT is a well-known therapeutic target.[10,11]

We utilised a bioengineered model to investigate the effects of glycosaminoglycan deposition and cyclic stretch on endothelial phenotypical changes, EndMT, and expression of inflammatory markers. Under static conditions, increased GAG concentrations in the extracellular matrix promoted the expression of both endothelial (CD31, vWF) and mesenchymal markers (MMP9, α-SMA). This suggests that higher GAG levels, in the absence of any tensile force, can create a microenvironment conducive to initiating an intermediate EndMT phenotype, characterised by the co-expression of both endothelial and mesenchymal markers.[11]

Previous studies have demonstrated that both low and atherogenic levels of shear stress, particularly in conjunction with glycosaminoglycan (GAG) enrichment and increased matrix stiffness, can promote endothelial-to-mesenchymal transition (EndMT).[51–55]

In our study, HAoVECs cultured in the stretch chamber were not exposed to shear stress; instead, they experienced cyclic tensile strain under controlled conditions. Despite the absence of flow-induced shear, our data show that GAG enrichment and the consequent increase in matrix stiffness, combined with reduced tensile strain, were sufficient to induce EndMT.

These findings suggest that endothelial cells utilize a convergent mechanosensory network that can integrate distinct mechanical inputs—including shear and tensile stress—within a pathological extracellular matrix environment. The observation of an inflammatory endothelial phenotype in our model further supports the idea that both types of biomechanical cues, when coupled with matrix stiffening and inflammatory signaling, can drive EndMT through shared pathways, such as TGF-β. Altogether, our work highlights the importance of matrix composition and tensile stress in modulating endothelial responses, and underscores the broader relevance of distinct yet overlapping mechanical forces in vascular pathophysiology.

Endothelial cells are mechanosensitive and cyclic tensile strain, experienced by valvular cells as cyclic stretch during the cardiac cycle, is a key mechanical force acting on the aortic valve and plays a crucial role in maintaining the endothelial phenotype.[23,27,56–60] Under healthy conditions, aortic valve leaflets experience approximately 10% cyclic stretch, while 15% and 20% cyclic stretch indicate hypertensive and severely hypertensive states, respectively. Additionally, aged and calcified regions experience reduced cyclic stretch, particularly in late-stage CAVD, which can approach 0% stretch.[24] Interestingly, our results show that both 10% and 20% cyclic stretch reduced EndMT marker expression compared to static conditions, suggesting that

mechanical stress helps preserve the endothelial phenotype. However, the total MMP activity of HAoVECs cultured on ColMA and hydrogels with high HA deposition (10 mg ml^{-1}) displayed no significant differences, indicating that while HA may influence the expression of specific mesenchymal markers such as MMP9, it does not necessarily alter overall MMP activity in this system.

We also examined the effects of cyclic stretch and GAG deposition on endothelial inflammation and leukocyte adhesion. Endothelial inflammation and dysfunction are key contributors to the progression of CAVD, as they facilitate the adhesion and transmigration of inflammatory cells into the subendothelial space, where they contribute to tissue remodelling and calcification.[20] Here, GAG deposition alone had a minimal impact on THP-1 adhesion under static conditions. However, 10% cyclic stretch significantly reduced ICAM-1 expression and leukocyte adhesion. In contrast, 20% stretch, particularly with high GAG concentrations, induced a pro-inflammatory response, evidenced by increased ICAM-1 expression and enhanced THP-1 adhesion.

To confirm our *in vitro* observations, we examined calcified aortic valve tissue surgically removed from CAVD patients undergoing prosthetic valve replacement, as well as control valve tissue obtained from deceased organ donors through our collaboration with the Australian Donor Tissue Biobank. The IHC results confirm the higher expression of CD31 in CAVD groups. Furthermore, the expression of MMP9 and α-SMA was higher in the endothelial layer of the CAVD group compared to the control, ultimately confirming our *in vitro* findings.

These observations reinforce the role of mechanical stress in perpetuating inflammation and disease progression in CAVD. Initial valve insults, such as congenital bicuspid valves or transient infections, may initiate abnormal ECM remodelling. Our findings provide a mechanism by which early ECM composition changes and reductions in cyclic stretch promote EndMT and leukocyte recruitment in a self-perpetuating cycle, resulting in gradual and inexorable CAVD disease progression.

In conclusion, we demonstrate that cyclic stretch and HA deposition determine EndMT and inflammation of endothelial cells. The physiological level of cyclic stretch reduces ICAM-1 expression and leukocyte adhesion, highlighting its protective role, while higher stretch intensities combined with GAGs promote a pro-inflammatory response (Fig. 7). These results highlight the importance of hemodynamic forces and matrix composition in regulating endothelial behaviour, offering insights into how mechanical and biochemical cues contribute to vascular inflammation and CAVD progression.

Data availability

All data supporting the findings of this study are presented within the manuscript and its ESI† files. Any additional information or inquiries can be directed to the corresponding author upon reasonable request.

Conflicts of interest

The authors declare no competing interests.

Acknowledgements

The authors sincerely thank the Australian Tissue bank and all the organ donors. This work was supported by an Ideas grant (GNT2020197) from the National Health and Medical Research Council (NHMRC) to S. B. and K. P., a L3 investigator grant to K. P., and Australian Government Research Training Program Scholarships to Y. M., M. K., and N. D.

References

1 V. T. Nkomo, J. M. Gardin, T. N. Skelton, J. S. Gottdiener, C. G. Scott and M. Enriquez-Sarano, Burden of valvular heart diseases: a population-based study, *Lancet.*, 2006, **368**(9540), 1005–1011.
2 R. O. Bonow and P. Greenland, Population-Wide Trends in Aortic Stenosis Incidence and Outcomes, *Circulation*, 2015, **131**(11), 969–971.
3 B. Alushi, L. Curini, M. R. Christopher, H. Grubitzch, U. Landmesser, A. Amedei and A. Lauten, Calcific Aortic Valve Disease-Natural History and Future Therapeutic Strategies, *Front. Pharmacol.*, 2020, **11**, 685.
4 N. M. Rajamannan, F. J. Evans, E. Aikawa, K. J. Grande-Allen, L. L. Demer and D. D. Heistad, *et al.*, Calcific aortic valve disease: not simply a degenerative process: A review and agenda for research from the National Heart and Lung and Blood Institute Aortic Stenosis Working Group. Executive summary: Calcific aortic valve disease-2011 update, *Circulation*, 2011, **124**(16), 1783–1791.
5 M. Ersboll, P. J. Schulte, F. Al Enezi, L. Shaw, L. Køber and J. Kisslo, *et al.*, Predictors and Progression of Aortic Stenosis in Patients With Preserved Left Ventricular Ejection Fraction, *Am. J. Cardiol.*, 2015, **115**(1), 86–92.
6 G. Strange, S. Stewart, D. Celermajer, D. Prior, G. M. Scalia and T. Marwick, *et al.*, Poor Long-Term Survival in Patients With Moderate Aortic Stenosis, *J. Am. Coll. Cardiol.*, 2019, **74**(15), 1851–1863.
7 J. G. Díez, Transcatheter aortic valve implantation (TAVI): the hype and the hope, *Cardiovasc. Dis.*, 2013, **40**(3), 298–301.
8 S. Nathaniel, S. Saligram and A. L. Innasimuthu, Aortic stenosis: An update, *World J. Cardiol.*, 2010, **2**(6), 135–139.
9 P. R. Goody, M. R. Hosen, D. Christmann, S. T. Niepmann, A. Zietzer and M. Adam, *et al.*, Aortic Valve Stenosis, *Arterioscler., Thromb., Vasc. Biol.*, 2020, **40**(4), 885–900.
10 J. C. Kovacic, S. Dimmeler, R. P. Harvey, T. Finkel, E. Aikawa, G. Krenning and A. H. Baker, Endothelial to Mesenchymal Transition in Cardiovascular Disease: JACC State-of-the-Art Review, *J. Am. Coll. Cardiol.*, 2019, **73**(2), 190–209.

11 S. Piera-Velazquez and S. A. Jimenez, Endothelial to Mesenchymal Transition: Role in Physiology and in the Pathogenesis of Human Diseases, *Physiol. Rev.*, 2019, **99**(2), 1281–1324.
12 R. Halevi, A. Hamdan, G. Marom, M. Mega, E. Raanani and R. Haj-Ali, Progressive aortic valve calcification: three-dimensional visualization and biomechanical analysis, *J. Biomech.*, 2015, **48**(3), 489–497.
13 K. Balachandran, P. Sucosky, H. Jo and A. P. Yoganathan, Elevated cyclic stretch alters matrix remodeling in aortic valve cusps: implications for degenerative aortic valve disease, *Am. J. Physiol.*, 2009, **296**(3), H756–H764.
14 A. Arzani and M. R. K. Mofrad, A strain-based finite element model for calcification progression in aortic valves, *J. Biomech.*, 2017, **65**, 216–220.
15 J.-H. Chen, C. A. Simmons and D. A. Towler, Cell–Matrix Interactions in the Pathobiology of Calcific Aortic Valve Disease, *Circ. Res.*, 2011, **108**(12), 1510–1524.
16 R. B. Hinton, J. Lincoln, G. H. Deutsch, H. Osinska, P. B. Manning, D. W. Benson and K. E. Yutzey, Extracellular Matrix Remodeling and Organization in Developing and Diseased Aortic Valves, *Circ. Res.*, 2006, **98**(11), 1431–1438.
17 A. J. Scott, L. R. Simon, H. N. Hutson, A. M. Porras and K. S. Masters, Engineering the aortic valve extracellular matrix through stages of development, aging, and disease, *J. Mol. Cell. Cardiol.*, 2021, **161**, 1–8.
18 S. Sánchez-Esteban, M. Castro-Pinto, A. Cook-Calvete, P. Reventún, M. Delgado-Marín and L. Benito-Manzanaro, *et al.*, Integrin-Linked Kinase Expression in Human Valve Endothelial Cells Plays a Protective Role in Calcific Aortic Valve Disease, *Antioxidants*, 2022, **11**(9), 1736.
19 A. Harvey, A. C. Montezano and R. M. Touyz, Vascular biology of ageing-Implications in hypertension, *J. Mol. Cell. Cardiol.*, 2015, **83**, 112–121.
20 W. Broeders, S. Bekkering, S. El Messaoudi, L. A. B. Joosten, N. van Royen and N. P. Riksen, Innate immune cells in the pathophysiology of calcific aortic valve disease: lessons to be learned from atherosclerotic cardiovascular disease?, *Basic Res. Cardiol.*, 2022, **117**(1), 28.
21 F. Bonafè, M. Govoni, E. Giordano, C. M. Caldarera, C. Guarnieri and C. Muscari, Hyaluronan and cardiac regeneration, *J. Biomed. Sci.*, 2014, **21**(1), 100.
22 E. López-Ruiz, G. Jiménez, L. Álvarez de Cienfuegos, C. Antic, R. Sabata, J. A. Marchal and P. Gálvez-Martín, Advances of hyaluronic acid in stem cell therapy and tissue engineering, including current clinical trials, *Eur. Cells Mater.*, 2019, **37**, 186–213.
23 R. C. Gupta, R. Lall, A. Srivastava and A. Sinha, Hyaluronic Acid: Molecular Mechanisms and Therapeutic Trajectory, *Front. Vet. Sci.*, 2019, **6**, 192.
24 K. A. Queisser, R. A. Mellema and A. C. Petrey, Hyaluronan and Its Receptors as Regulatory Molecules of the Endothelial Interface, *J. Histochem. Cytochem.*, 2021, **69**(1), 25–34.
25 K. J. Rodriguez, L. M. Piechura and K. S. Masters, Regulation of valvular interstitial cell phenotype and function by hyaluronic acid in 2-D and 3-D culture environments, *Matrix Biol.*, 2011, **30**(1), 70–82.
26 J. A. Bramsen, B. R. Alber, M. Mendoza, B. T. Murray, M. H. Chen, P. Huang and G. J. Mahler, Glycosaminoglycans affect endothelial to mesenchymal transformation, proliferation, and calcification in a 3D model of aortic valve disease, *Front. Cardiovasc. Med.*, 2022, **9**, 975732.
27 S. Aguilera Suarez, N. C. Sekar, N. Nguyen, A. Lai, P. Thurgood and Y. Zhou, *et al.*, Studying the Mechanobiology of Aortic Endothelial Cells Under Cyclic Stretch Using a Modular 3D Printed System, *Front. Bioeng. Biotechnol.*, 2021, **9**, 791116.
28 B. Velasco-Rodriguez, T. Diaz-Vidal, L. C. Rosales-Rivera, C. A. García-González, C. Alvarez-Lorenzo and A. Al-Modlej, *et al.*, Hybrid Methacrylated Gelatin and Hyaluronic Acid Hydrogel Scaffolds. Preparation and Systematic Characterization for Prospective Tissue Engineering Applications, *Int. J. Mol. Sci.*, 2021, **22**(13), 6758.
29 X. Lan, Z. Ma, A. Dimitrov, M. Kunze, A. Mulet-Sierra and K. Ansari, *et al.*, Double crosslinked hyaluronic acid and collagen as a potential bioink for cartilage tissue engineering, *Int. J. Biol. Macromol.*, 2024, **273**, 132819.
30 S. P. Gennari, J. Mirković and M. C. Macdonald, Animacy and competition in relative clause production: a cross-linguistic investigation, *Cogn. Psychol.*, 2012, **65**(2), 141–176.
31 D. E. Discher, P. Janmey and Y. L. Wang, Tissue cells feel and respond to the stiffness of their substrate, *Science*, 2005, **310**(5751), 1139–1143.
32 J. P. Gong, Why are double network hydrogels so tough?, *Soft Matter*, 2010, **6**(12), 2583–2590.
33 S. Baratchi, K. Khoshmanesh, O. L. Woodman, S. Potocnik, K. Peter and P. McIntyre, Molecular Sensors of Blood Flow in Endothelial Cells, *Trends Mol. Med.*, 2017, **23**(9), 850–868.
34 C. A. Dessalles, C. Leclech, A. Castagnino and A. I. Barakat, Integration of substrate- and flow-derived stresses in endothelial cell mechanobiology, *Commun. Biol.*, 2021, **4**(1), 764.
35 S. Noria, F. Xu, S. McCue, M. Jones, A. I. Gotlieb and B. L. Langille, Assembly and reorientation of stress fibers drives morphological changes to endothelial cells exposed to shear stress, *Am. J. Pathol.*, 2004, **164**(4), 1211–1223.
36 Y. Zhou, N. C. Sekar, P. Thurgood, S. Needham, K. Peter, K. Khoshmanesh and S. Baratchi, Bioengineered Vascular Model of Foam Cell Formation, *ACS Biomater. Sci. Eng.*, 2023, **9**(12), 6947–6955.
37 K. J. Rodriguez, L. M. Piechura, A. M. Porras and K. S. Masters, Manipulation of valve composition to elucidate the role of collagen in aortic valve calcification, *BMC Cardiovasc. Disord.*, 2014, **14**(1), 29.
38 A. M. Porras, J. A. Westlund, A. D. Evans and K. S. Masters, Creation of disease-inspired biomaterial environments to mimic pathological events in early calcific aortic valve disease, *Proc. Natl. Acad. Sci. U. S. A.*, 2018, **115**(3), E363–E371.
39 C. Qian, G. Dong, C. Yang, W. Zheng, C. Zhong and Q. Shen, *et al.*, Broadening horizons: molecular mechanisms and

disease implications of endothelial-to-mesenchymal transition, *Cell Commun. Signaling*, 2025, **23**(1), 16.
40 M. S. Hulshoff, X. Xu, G. Krenning and E. M. Zeisberg, Epigenetic Regulation of Endothelial-to-Mesenchymal Transition in Chronic Heart Disease, *Arterioscler., Thromb., Vasc. Biol.*, 2018, **38**(9), 1986–1996.
41 S. M. Evrard, L. Lecce, K. C. Michelis, A. Nomura-Kitabayashi, G. Pandey and K. R. Purushothaman, *et al.*, Endothelial to mesenchymal transition is common in atherosclerotic lesions and is associated with plaque instability, *Nat. Commun.*, 2016, **7**(1), 11853.
42 W. Jia, Z. Wang, C. Gao, J. Wu and Q. Wu, Trajectory modeling of endothelial-to-mesenchymal transition reveals galectin-3 as a mediator in pulmonary fibrosis, *Cell Death Dis.*, 2021, **12**(4), 327.
43 G. J. Mahler, E. J. Farrar and J. T. Butcher, Inflammatory cytokines promote mesenchymal transformation in embryonic and adult valve endothelial cells, *Arterioscler., Thromb., Vasc. Biol.*, 2013, **33**(1), 121–130.
44 G. A. Cabral-Pacheco, I. Garza-Veloz, C. Castruita-De la Rosa, J. M. Ramirez-Acuña, B. A. Perez-Romero and J. F. Guerrero-Rodriguez, *et al.*, The Roles of Matrix Metalloproteinases and Their Inhibitors in Human Diseases, *Int. J. Mol. Sci.*, 2020, **21**(24), 9739.
45 N. F. Jufri, A. Mohamedali, A. Avolio and M. S. Baker, Mechanical stretch: physiological and pathological implications for human vascular endothelial cells, *Vasc. Cell*, 2015, **7**, 8.
46 K. Fujiwara, Mechanical stresses keep endothelial cells healthy: beneficial effects of a physiological level of cyclic stretch on endothelial barrier function, *Am. J. Physiol.*, 2003, **285**(4), L782–L784.
47 K. J. Choi, J.-K. Nam, J.-H. Kim, S.-H. Choi and Y.-J. Lee, Endothelial-to-mesenchymal transition in anticancer therapy and normal tissue damage, *Exp. Mol. Med.*, 2020, **52**(5), 781–792.
48 J. Bischoff, Endothelial-to-Mesenchymal Transition, *Circ. Res.*, 2019, **124**(8), 1163–1165.
49 I. F. Hall, F. Kishta, Y. Xu, A. H. Baker and J. C. Kovacic, Endothelial to mesenchymal transition: at the axis of cardiovascular health and disease, *Cardiovasc. Res.*, 2024, **120**(3), 223–236.
50 D. Medici and R. Kalluri, Endothelial-mesenchymal transition and its contribution to the emergence of stem cell phenotype, *Semin. Cancer Biol.*, 2012, **22**(5–6), 379–384.
51 S. Dahal, P. Huang, B. T. Murray and G. J. Mahler, Endothelial to mesenchymal transformation is induced by altered extracellular matrix in aortic valve endothelial cells, *J. Biomed. Mater. Res., Part A*, 2017, **105**(10), 2729–2741.
52 S. Dahal, J. A. Bramsen, B. R. Alber, B. T. Murray, P. Huang, M. H. Chen and G. J. Mahler, Chondroitin Sulfate Promotes Interstitial Cell Activation and Calcification in an In Vitro Model of the Aortic Valve, *Cardiovasc. Eng. Technol.*, 2022, **13**(3), 481–494.
53 S. G. Mina, P. Huang, B. T. Murray and G. J. Mahler, The role of shear stress and altered tissue properties on endothelial to mesenchymal transformation and tumor-endothelial cell interaction, *Biomicrofluidics*, 2017, **11**(4), 044104.
54 S. G. Mina, W. Wang, Q. Cao, P. Huang, B. T. Murray and G. J. Mahler, Shear stress magnitude and transforming growth factor-βeta 1 regulate endothelial to mesenchymal transformation in a three-dimensional culture microfluidic device, *RSC Adv.*, 2016, **6**(88), 85457–85467.
55 M. Mendoza, M.-H. Chen, P. Huang and G. J. Mahler, Shear and endothelial induced late-stage calcific aortic valve disease-on-a-chip develops calcium phosphate mineralizations, *Lab Chip*, 2022, **22**(7), 1374–1385.
56 N. Chandra Sekar, K. Khoshmanesh and S. Baratchi, Bioengineered models of cardiovascular diseases, *Atherosclerosis*, 2024, **393**, 117565.
57 G. Concilia, A. Lai, P. Thurgood, E. Pirogova, S. Baratchi and K. Khoshmanesh, Investigating the mechanotransduction of transient shear stress mediated by Piezo1 ion channel using a 3D printed dynamic gravity pump, *Lab Chip*, 2022, **22**(2), 262–271.
58 A. Lai, A. Hawke, M. Mohammed, P. Thurgood, G. Concilia and K. Peter, *et al.*, A microfluidic model to study the effects of arrhythmic flows on endothelial cells, *Lab Chip*, 2024, **24**(8), 2347–2357.
59 A. Lai, P. Thurgood, C. D. Cox, C. Chheang, K. Peter and A. Jaworowski, *et al.*, Piezo1 Response to Shear Stress Is Controlled by the Components of the Extracellular Matrix, *ACS Appl. Mater. Interfaces*, 2022, **14**(36), 40559–40568.
60 A. Lai, Y. Zhou, P. Thurgood, C. Chheang, N. Chandra Sekar and N. Nguyen, *et al.*, Endothelial Response to the Combined Biomechanics of Vessel Stiffness and Shear Stress Is Regulated via Piezo1, *ACS Appl. Mater. Interfaces*, 2023, **15**(51), 59103–59116.